Accepted in: Phys. Status Solidi A (2017)

From large-size to micro-LEDs: scaling trends revealed by modeling

Sergey S. Konoplev, Kirill A. Bulashevich, and Sergey Yu. Karpov *

STR Group – Soft-Impact, Ltd., P.O.Box 83, 27 Engels av., St.Petersburg, 194156 Russia

Keywords LEDs, micro-LEDs, scaling, chip design, efficiency, simulation

General trends in scaling dimensions of a circular-shaped flip-chip light-emitting diode (LED) are studied by coupled electrical-thermal-optical simulations. Advanced chip design is considered, providing high efficiency of light extraction through the top surface of the LED die. The simulation model accounts for such important effects, as current crowding near metallic electrodes, thermal and non-thermal efficiency droop caused by Auger recombination, and surface recombination at the edges of the LED active region. Interplay and competition of the mechanisms is demonstrated in a wide range of operating current densities and chip dimensions varied from tens to hundreds of micrometers. It is shown that surface recombination, which is especially important in small-size LEDs, is the major mechanism controlling evolution of the LED characteristics under the chip size variation. The impact of surface recombination on LED characteristics is predicted to weaken at high current densities typical for operation of micro-LEDs due to shortening of carrier life time in the active region. Advantages of micro-LEDs are discussed on the basis of the simulations.

Preprint 2017

1 Introduction Currently, there is a big interest to development of efficient InGaN-based and AlGaInP-based micro-LEDs for various applications: high-resolution miniature displays, medical and biological imaging and sensing, non-contact lithography, augmented reality, and, in a distant prospect, visible-light communication (see [1-4] and references therein). In contrast to large-size high-power devices, micro-LEDs operate typically at high current densities, up to ~1-5 kA/cm^2 [4-6]. Under such conditions, strong thermal and non-thermal droop of LED efficiency caused by Auger recombination are expected to limit substantially the device performance. Besides, surface recombination at the edges of active region [7] may produce additional carrier losses in small-size LEDs. Scaling of LED dimensions results in size-controlled interplay of various mechanisms affecting the emission efficiency. In particular, carrier losses caused by surface recombination depend essentially on the size of LED chip, as well as current crowding leading to enhanced efficiency droop in the regions of strong current localization. On the other hand, the length of ambipolar carrier diffusion in the LED active region, affecting the strengths of both surface recombination and current crowding, is largely dependent on non-equilibrium carrier density and, hence, on the current density chosen for the device operation. Therefore, any improvement of small-size LED efficiency requires coupled optimization of the device structure, chip design, and its operating conditions.

This paper reports on the simulation study aimed at better understanding of general trends in evolution of main LED characteristics and efficiency under reduction of the LED size. For this purpose, coupled electrical, thermal, and optical models [7,8] have been applied, which is important in view of interplay between the above phenomena.

2 Heterostructure and chip design We consider a blue LED structure (440 nm) consisting of undoped five-period $In_{0.18}Ga_{0.82}N$/GaN multiple-quantum well (MQW) and $Al_{0.15}Ga_{0.85}N$ electron blocking layer sandwiched between n-GaN and p-GaN cladding layers (detailed specification is given in Table 1). The structure design is close, for example, to those reported in [9,10]. Here, acceptor concentration in the last GaN barrier was assumed to rise linearly from zero to 2×10^{19} cm^{-3} because of Mg back diffusion from p-type layers during growth of the structure [11].

* Corresponding author: sergey.karpov@str-soft.com, Phone: +7 812 554 4570, Fax: +7 812 326 6194

Electron mobility of 100 $cm^2/V \cdot s$ and hole mobility of 10 $cm^2/V \cdot s$ were assumed for all the layers. In InGaN/GaN MQW, the electron and hole non-radiative lifetimes of ~20 ns and ~500 ns, respectively, the radiative recombination coefficient $B_0 = 2.1 \times 10^{-11}$ cm^3/s, and the Auger recombination coefficients $C_n = C_p = 4.5 \times 10^{-31}$ cm^3/s provided maximum internal quantum efficiency (IQE) of 81% at room temperature and current density of ~0.3 A/cm^2.

Table 1 LED heterostructure (from bottom to top).

Layer	Thickness, nm	Doping, cm^{-3}
n-GaN cladding layer	5000	5×10^{18}
5×(2.7 nm InGaN/7 nm GaN) MQW	41.5	undoped
p-GaN last barrier	8	$0\text{-}2 \times 10^{19}$
p-AlGaN electron blocking layer	20	2×10^{19}
p-GaN cladding layer	180	5×10^{19}

All the recombination coefficients are generally temperature-dependent, producing thermal IQE droop. Because of lacking consistent experimental information on their typical temperature dependence, we accounted for thermal droop in a simplified manner: the electron and hole non-radiative life times and both Auger recombination coefficients were assumed to be independent of temperature T, whereas the radiative recombination coefficient obeyed the relationship $B(T) = B_0(T/300\ \mathrm{K})^{-3/2}$ specific for bulk materials. This resulted in maximum IQE reduction down to 68%, 56%, and 46% at 400 K, 500 K and 600 K, respectively. Despite the simplified accounting for the temperature dependence of recombination coefficients, our model predicts quantitatively well (~11%) the thermal IQE droop of ~12% measured in a similar MQW LED structure at 85°C and current density of 83 A/cm^2 [12].

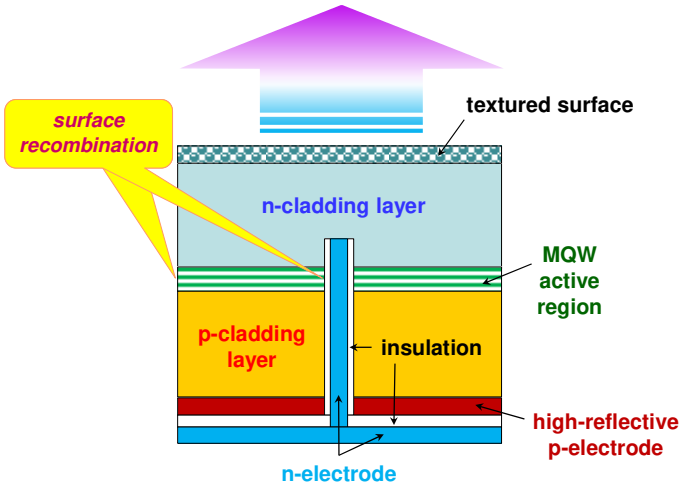

Figure 1 Schematic LED chip design (cross-section). Arrow indicates the dominant pathway of light emission.

Design of circular flip-chip LED chosen for simulations is shown schematically in Fig.1. It contains a continuous Ag-based highly reflective p-electrode formed to p-GaN cladding layer and a columnar Au-based n-electrode providing current access to the n-GaN cladding layer through a cylindrical aperture etched inside the structure. We assume the substrate to be removed after growing the LED structure and a texture to be formed on the back side of the n-GaN cladding layer to enhance light extraction from the die.

Actually, the above design is borrowed from the UX:3 chips developed by Osram OS [13] with the difference that a single columnar n-electrodes were exploited in the LED dice examined in our study. The major advantage of the design is high light extraction efficiency (LEE) achieved due to absence of any metallic electrodes on the emitting surface of LED die that may shade emitted light. In the presence of metallic electrodes on the emitting surface, current crowding combined with the shading effect may produce LEE decreasing with current, which contributes additionally to the LED efficiency droop [14].

Three-dimensional (3D) modelling of LED operation was carried out with the SimuLED package [15] implementing the hybrid approach suggested in [16]. The approach considered self-consistently current spreading and heat transfer in the LED dice with account of temperature-dependent activation of donors and acceptors, which is especially important for p-GaN contact layers, and temperature-dependent materials parameters like energy gaps, effective densities of states in the conduction and valence band, etc. The lateral carrier transport in the InGaN QWs and surface recombination effects were taken into account by the model described in [7].

In order to investigate into the scaling trends, the outer diameter of the LED chip (D) was varied from 16 μm to 300 μm, while the aperture diameter of 10 μm was kept unchanged. Specific resistances of both n- and p-contacts were chosen to be of 3×10^{-4} Ω·cm^2. Heat removal from the LED die through its bottom surface was simulated with the heat-transfer coefficient of 10 W/cm^2·K.

Surface recombination velocity of 10^3 cm/s and ambipolar carrier diffusivity in InGaN active region of 2 cm^2/s were chosen for our simulations (see [7] for comments on the choice of these parameters). Surface recombination on both aperture and side walls of the chip was taken into account (see Fig.1).

Light extraction from the LED dice was simulated by 3D ray tracing using typically 10^7 probe rays and accounting for current-dependent distribution of the emission intensity across the LED active region coming from electrical-thermal modelling. Similarly to [14], texturing of the n-cladding layer surface was modelled with close-packed array of hexagonal pyramids with the period of 500 nm and height-to-base ratio of four.

3 Results and discussion

3.1 Light extraction efficiency Ray-tracing analysis has shown the emitted photons to be largely extracted through the textured surface of LED dice (see Fig.1). LEE of 85±1% to the top hemisphere and 89±1% to all directions predicted for an immersion medium with the refractive index of 1.5 is found to depend neither on operating current density nor on the chip size. This is consequence of absence of any metallic electrodes on the top emitting surface of the die and strong scattering of light by the surface texture. The obtained LEE agree well to that calculated for 1×1 mm^2 UX:3 chip with the same immersion medium, which is the evidence for good scalability of the chosen chip design in view of the efficiency of light extraction.

3.2 Current density-voltage characteristics In order to compare LEDs of various sizes, it is reasonable to analyze their characteristics as a function of mean current density J, which is the ratio of current flowing through device to the total active region area.

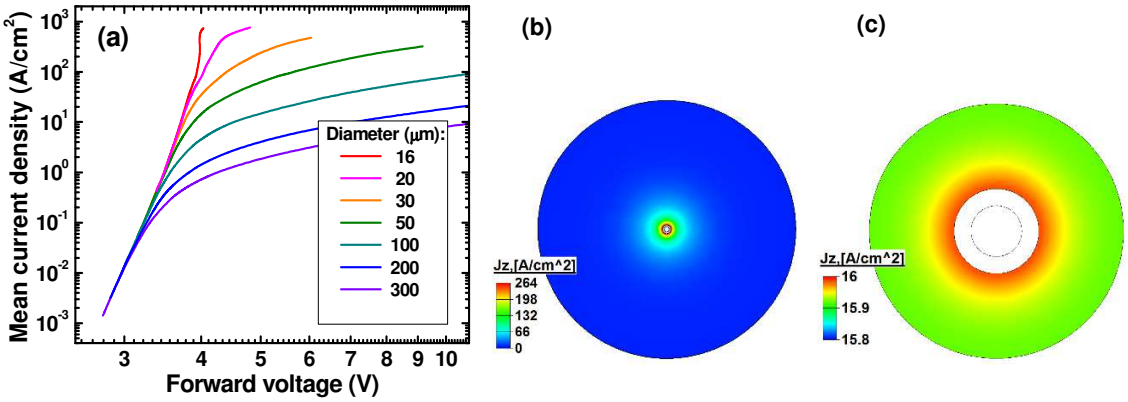

Figure 2 Current density-voltage characteristics of LEDs with various outer diameters (a) and distributions of current density in the active region of LED with the diameter of (b) 300 μm at 10 mA and (c) 30 μm at 0.1 mA (in both cases, mean current density is about 16 A/cm^2).

Figure 2a shows the current density-voltage (J-V) characteristics of LEDs with various outer diameters D. At the current densities less than ~0.1 A/cm^2, all the J-V curves merge, which is expectable for devices pumped by current uniformly distributed over the active region. At higher current densities, the

exponential rise of the current density with voltage changes to a gradual variation controlled by LED specific series resistances, i.e. the resistance calculated per unit area. The changes start at lower current densities in the LEDs of larger sizes. This fact requires special interpretation, as, at a glimpse, the specific series resistance is determined by only the LED structure design and should be independent of the chip lateral size.

Local current density distributions over the active regions of LEDs with D = 300 μm (Fig.2b) and 30 μm (Fig.2c) are compared in Figs.2b,c. Both distributions correspond to nearly the same mean current density of about 16 A/cm^2. One can see that the distribution in the large-size LED (Fig.2b) is extremely non-uniform with the peak current density approaching ~260 A/cm^2 at the border of the n-contact aperture. This is manifestation of strong current crowding in the LED die, which is absent in small-size LEDs (Fig.2c). Similarly to the cases discussed in [16], the current crowding was found to be controlled by the electric conductivity and thickness of the n-GaN contact layers.

In the case of strong current crowding, the specific series resistance is controlled by the area of current localization rather than by the total area of the active region. Since the chip size reduction suppresses current crowding, as it can be seen from comparison of Fig.2b and Fig.2c, the specific resistance becomes size-dependent, increasing with the LED dimensions. This explains why the contribution of series resistance to the J-V characteristic is predicted to start at lower current densities in large-size LEDs.

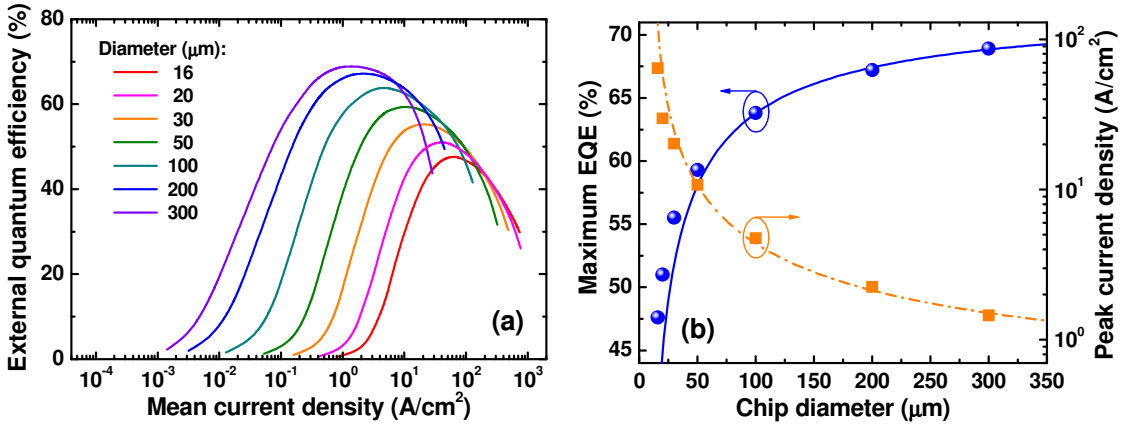

Figure 3 EQEs of LEDs with various outer diameters as a function of mean current density (a). Maximum EQE value and peak current density *versus* outer chip diameter (b); symbols are results of simulations, lines are fitting curves (see text for more detail).

3.3 Emission efficiency External quantum efficiencies (EQEs) as a function of mean current density simulated for LEDs of various sizes are compared in Fig.3a. These curves correspond to the heat sink temperature of 300 K but account self-consistently for the LED self-heating enhanced at high current densities. Modelling of the LED structure, which is the same in all the devices, has shown that electron leakage to p-side of the structure is negligible at temperatures up to 600 K. As LEE (η_{ext}) is found to be independent of the current density (see Sec.3.1), the variation of LED efficiency with current should be attributed entirely to that of IQE.

Simulations predict two main trends in the EQE variation under decreasing LED outer diameter: (i) reduction of maximum (peak) EQE value and (ii) increase of the peak current density at which the maximum EQE is achieved. Both trends agree qualitatively with experimental ones reported in [5,17].

The predicted maximum EQE values and peak current densities are plotted in Fig.3b by symbols *versus* outer chip diameter. In order to interpret the predicted trends, we invoke a simplified ABC-model describing carrier recombination in the LED active region in terms of Shockley-Read-Hall non-radiative recombination at point/extended defects (with the recombination coefficient A), radiative recombination (with the recombination coefficient B), and Auger recombination (with the recombination coefficient C). Surface recombination can be roughly accounted for in the model by adding the term $A' = S\mathcal{P}/\Sigma$ to the

coefficient A [18], where S is the surface recombination velocity, $\mathcal{P} = \pi(D+d)$ and $\Sigma = \frac{1}{4}\pi(D^2 - d^2)$ are the active region perimeter and area, respectively, and d is the aperture diameter. Introducing the Q-factor (see, for example, [19])

$$Q = B/\sqrt{(A+A')C} = Q_\infty/[1+\delta/(D-d))]^{1/2} \quad , \tag{1}$$

where $Q_\infty = B/(AC)^{1/2}$ is the Q-factor of a large-size LED in which surface recombination is negligible ($D \to \infty$) and $\delta = 4S/A$, one can calculate the maximum EQE value as $\mathrm{EQE}_{\max} = \eta_{ext} Q/(Q+2)$. Fitting of the maximum EQE values obtained by simulations with the above expressions and parameters $\eta_{ext} = 89\%$, $Q_\infty = 8.6$, and $\delta = 170$ μm (solid line in Fig.3b), provides a reasonable agreement between the numerical modelling and crude ABC-model.

On the other hand, the peak current density J_p, at which the LED efficiency approaches its maximum value, can be approximated by ABC-model as follows:

$$J_p = J_\infty[1+\delta/(D-d)]\,\frac{Q_\infty + 2\sqrt{1+\delta/(D-d)}}{Q_\infty + 2} \tag{2}$$

Here, J_∞ is the peak current density in large-size LED ($D \to \infty$) and other parameters have the same meaning, as previously. Equation (2) fits well the results of numerical simulations at J_∞=0.5 A/cm^2, $Q_\infty = 8.6$, and $\delta = 530$ μm (see the dash-dotted line in Fig.3b). The fact that fitting of simulated maximum EQEs and peak current densities provides very different values of δ is the evidence for inapplicability of the simplified ABC-model for quantitative prediction of the LED characteristics evolution under changing their dimensions. Nevertheless, the model catches qualitatively the general scaling trends.

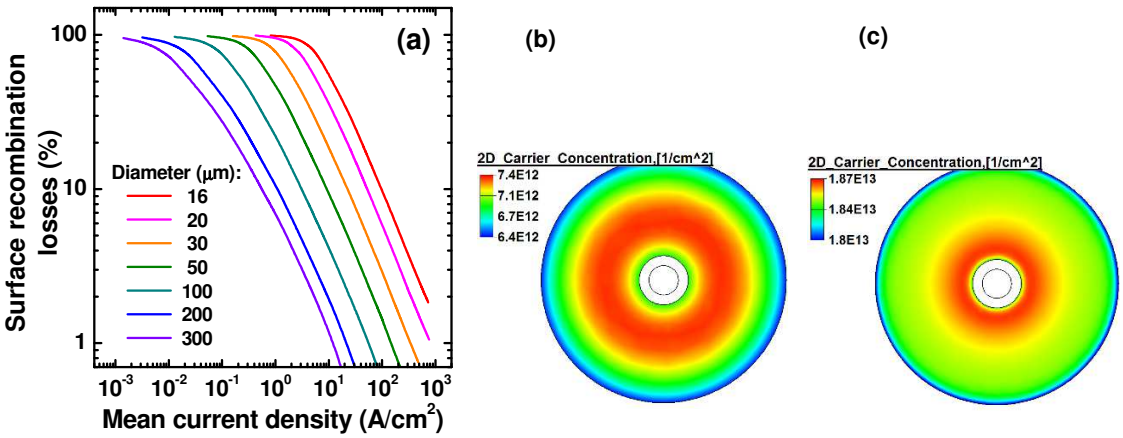

Figure 4 Current density-voltage characteristics of LEDs with various outer diameters (a) and distributions of current density in the active region of LED with the diameter of (b) 300 μm at 10 mA and (c) 30 μm at 0.1 mA (in both cases, mean current density is about 16 A/cm^2).

The above analysis demonstrates the scaling trends to be largely determined by surface recombination at the active region edges. In order to highlight the role of this mechanism, we have plotted in Fig.4a the percentage of surface recombination losses (the ratio of surface recombination current to the total current flowing though the diode) *versus* current density simulated for LEDs of various sizes. The figure reveals two main tendencies. One is reduction of surface-recombination losses with the current density. This can be explained by shortening of non-equilibrium carrier life time in the active region and subsequent decrease of their ambipolar diffusion length which controls the "dead" areas at the active region edges (see Fig.4b,c) where surface recombination is valuable [7]. The second tendency is decrease in the surface-recombination losses with the LED chip size, which is expectable because of the ratio of the above "dead" area to the total area of the active region decreasing with the chip dimensions.

One more important observation coming from Fig.3a is that EQE of small-size LEDs can exceed the efficiency of large-size devices at high current densities. The mechanism behind this phenomenon is size-dependent current crowding. In large LEDs, current crowding is strong, producing regions where local current density is much greater than the mean current density in the diode (see Fig.2b). Here, Auger recombination is remarkably enhanced, resulting in a strong non-thermal efficiency droop. In contrast, current crowding is suppressed in small-size LEDs and the local current density is close to the mean one. Therefore, the efficiency droop starts to occur at considerably higher current densities.

3.4 Electrical efficiency Figure 5a shows simulated wall-plug efficiencies (WPEs) of LEDs with various outer diameters as a function of current density. Similarly to EQE, the maximum WPE values decline and the current density corresponding to this maximum increase at smaller chip dimensions. The predicted WPE values are generally less than the EQE values at the same current density, which is related to dissipation of electric power in the bulk of the device via self-heating. In order to characterize the additional "electrical" losses, we have plotted in Fig.5b the relative difference between EQE and WPE of the LEDs. The figure shows that the curve corresponding to D = 16 μm serves actually as the envelope for all other curves that start to deviate drastically from the envelope at the current densities dependent on the chip size. The deviations correlate well with the changes in the slope of J-V characteristics (see Fig.2a). Therefore, the rise in the "electrical" losses compared to those of the envelope can be attributed to increasing Joule losses caused by size-dependent specific series resistances of the LEDs.

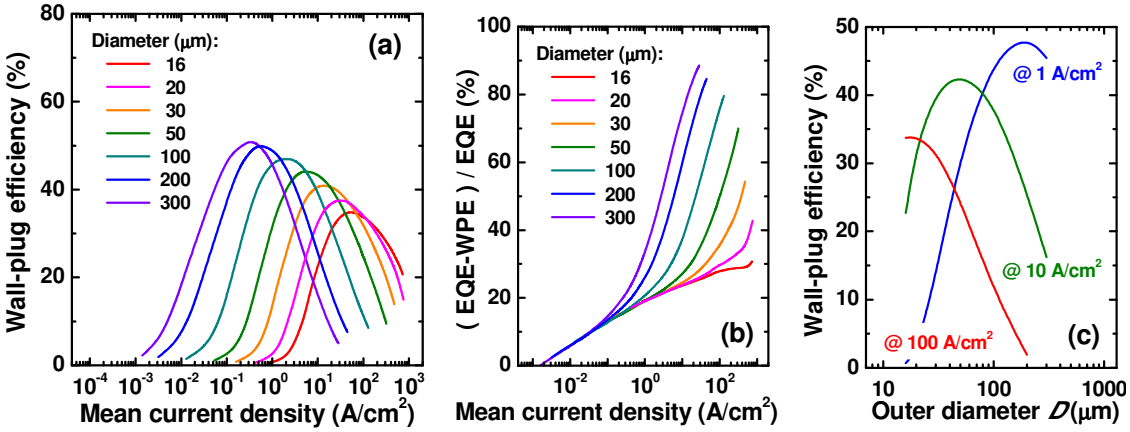

Figure 5 WPEs (a) and "electrical" losses (b) of LEDs with various outer diameters as a function of mean current density. Dependence of WPE on the LED size for the fixed current densities of 1, 10, and 100 A/cm^2 (c).

Comparison of the "electrical" losses in LEDs of various dimensions leads to important conclusion that the losses decrease substantially when the chip size is reduced.

It is interesting that interplay between the "electrical" losses, efficiency droop at high current densities, and current crowding results in non-monotonous dependence of WPE on the LED size at a given operating current density (see Fig.5c). As soon as the operating current density is chosen from some requirements, the LED dimensions should be carefully optimized in order to get maximum WPE.

3.5 LED self-heating Figure 6a displays the simulated average temperature of the active region *versus* mean current density for LED of various sizes. According to the results, the temperature grows dramatically with the chip diameter at a given current density. The explanation of such a behaviour is similar to that used in analysis of J-V characteristics (see Sec.3.2). Because of current crowding, the current density is localized near the columnar n-electrode, resulting also in a similar localization of the heat release and non-uniform temperature distribution in the active region (see Figs.6b,c). As a result of the chip-size dependent current crowding, the specific thermal resistance grows with the LED size, leading to more intensive self-heating of large-size devices. The latter conclusion is in qualitative agreement with the data of [20] reported for near-UV micro-pixel LED arrays.

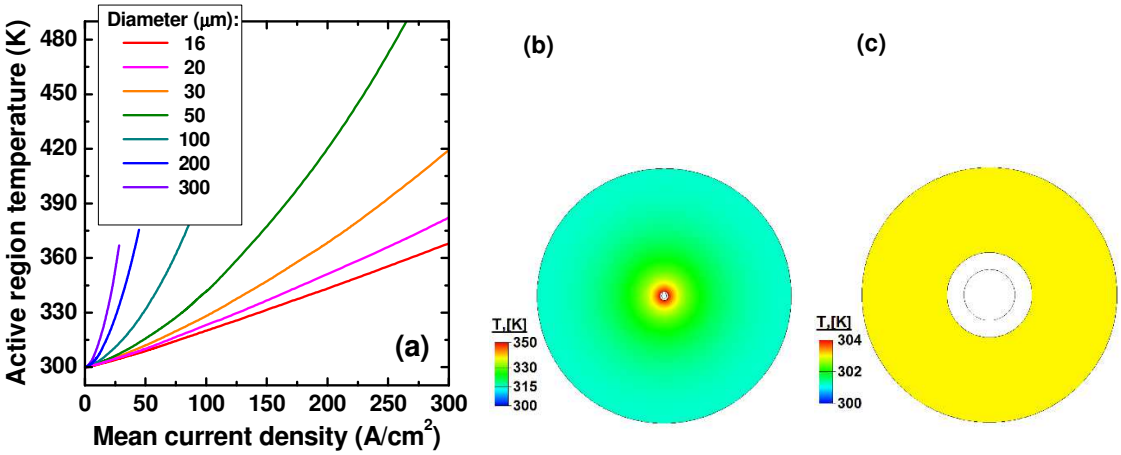

Figure 6 Average active region temperature of LED with various outer diameters as a function of mean current density (a) and temperature distributions in the active region of LED with the diameter of (b) 300 μm at 10 mA and (c) 30 μm at 0.1 mA (in both cases, mean current density is about 16 A/cm^2).

Our model does not consider coupled heat transfer in the LED dice and a bulky heat sink. Accounting for the heat removal from the dice via heat-transfer coefficient is quite acceptable for micro-LEDs operating within an LED array. In the case of a single LED, however, the lateral heat transfer in the bulk of the heat sink may reduce the temperature non-uniformity over the LED active region and, thus, lower the predicted active region overheating in large-size LEDs. The use of the coupled thermal simulations of both LED die and a particular heat sink enables in this case more accurate predictions of the device overheating.

4 Conclusions Using numerical simulations, we have studied general trends in evolution of main LED characteristics under scaling their dimensions. The evolution is found to be controlled by size-dependent interplay of such important mechanisms, as current crowding, surface recombination at the active region edges, LED self-heating, and non-thermal efficiency droop caused by Auger recombination.

The J-V characteristics of LEDs are turned out to be determined by size-dependent specific series resistances increasing substantially in large-size devices because of more pronounced current crowding.

When the chip dimensions are reduced, the maximum EQE and WPE values are predicted to decline and the current densities corresponding to the efficiency maximum are found to increase, in line with characterization data available in literature. Both trends can be explained by size-dependent contribution of surface recombination to the carrier losses. This contribution rises when the LED chip size is decreased and weakens at high operating current densities due to shortening of non-equilibrium carrier life time in the active region. Because of interplaying mechanisms, both EQE and WPE may depend non-monotonically on the chip dimensions, if the operating current is *a priori* chosen by some requirements. Under these conditions, the chip size and its design should be carefully optimized to get maximum LED efficiency.

In view of dramatic impact of surface recombination on the efficiency of small-size light emitters, passivation of the active region edges aimed at reducing the surface recombination velocity seem to become a critical stage of the micro-LED fabrication technology.

Being compared at a relatively high operating current density, micro-LEDs are found to be advantageous over the large-size devices in providing (i) lower “electrical” losses, i.e. smaller difference between EQE and WPE values, and (i) lower device self-heating. Both effects are related to suppression of current crowding in small-size devices.

The chip design considered in our study seems to be quite promising for micro-LED fabrication, since it is well-scalable, providing a high efficiency of light extraction independent of the LED size and operating current density.

Our study demonstrates that modelling of micro-LED operation is a helpful and powerful tool for optimization of its heterostructure and chip design. Further development of the relevant models is, however, required with the focus on temperature dependence of recombination parameters which are yet known with insufficient accuracy. For this purpose, experimental information on recombination coefficients and surface recombination velocities at various facets of LED dice is highly demanded.

References

[1] H. Xu, J. Zhang, K. M. Davitt, Y.-K. Song, and A. V. Nurmikko, J. Phys. D: Appl. Phys. **41**, 094013 (2008).

[2] H. X. Jiang and J. Y. Lin, Optics Express **21**, A475 (2013).

[3] J. J. D. McKendry, D. Massoubre, S. Zhang, B. R. Rae, R. P. Green, E. Gu, R. K. Henderson, A. E. Kelly, and M. D. Dawson, J. Lightwave Technol. **30**, 61 (2012).

[4] J. R. Bonar, G. J. Valentine, Zheng Gong, J. Small, S. Gorton, Proc. SPIE **9768**, 97680Y-1 (2016).

[5] P. Tian, J. J. D. McKendry, Z. Gong, B. Guilhabert, I. M. Watson, E. Gu, Z. Chen, G. Zhang, and M. D. Dawson, Appl. Phys. Lett. **101**, 231110 (2012).

[6] J. Herrnsdorf, J. J. D. McKendry, S. Zhang, E. Xie, R. Ferreira, D. Massoubre, A. M. Zuhdi, R. K. Henderson, I. Underwood, S. Watson, A. E. Kelly, E. Gu, and M. D. Dawson, IEEE Trans. Electron. Dev. **62**, 1918 (2015).

[7] K. A. Bulashevich and S. Yu. Karpov, Phys. Stat. Solidi RRL **10**, 480 (2016).

[8] M. V. Bogdanov, K. A. Bulashevich, I. Yu. Evstratov, A. I. Zhmakin, and S. Yu. Karpov, Semicond. Sci. Technol. **23**, 125023 (2008).

[9] Jun-Youn Kim, Youngjo Tak, Jaekyun Kim, Hyun-Gi Hong, Suhee Chae, Jae Won Lee, Hyoji Choi, Youngsoo Park, U-In Chung), Jong-Ryeol Kim, and Jong-In Shim, Proc. SPIE **8262**, 82621D (2012).

[10] C. X. Ren, B. Rouet-Leduc, J. T. Griffiths, E. Bohacek, M. J. Wallace, P. R. Edwards, M. A. Hopkins, D. W. E. Allsopp, M. J. Kappers, R. W. Martin, and R. A. Oliver, Superlattices and Microstructures **99**, 118 (2016).

[11] L. Kirste, K. Köhler, M. Maier, M. Kunzer, M. Maier, and J. Wagner, J. Mater. Sci.: Mater. Electron. **19**, S176 (2008).

[12] A. Nirschl, A. Gomez-Iglesias, M. Sabathil, G. Hartung, and J. Off, and Dominique Bougeard, Phys. Stat. Solidi A **210**, 2509 (2014).

[13] B. Hahn, B. Galler, and K. Engl, Jpn. J. Appl. Phys. **53**, 100208 (2014).

[14] M. V. Bogdanov, K. A. Bulashevich, O. V. Khokhlev, I. Yu. Evstratov, M. S. Ramm, and S. Yu. Karpov, Phys. Stat. Solidi C **7**, 2124 (2010).

[15] http://www.str-soft.com/products/SimuLED/index.htm

[16] M. V. Bogdanov, K. A. Bulashevich, I. Yu. Evstratov, A. I. Zhmakin, and S. Yu. Karpov, Semicond. Sci. Technol. **23**, 125023 (2008).

[17] Shen-Che Huang, Heng Li, Zhe-Han Zhang, Hsiang Chen, Shing-Chung Wang, and Tien-Chang Lu, Appl. Phys. Lett. **110**, 021108 (2017).

[18] P. Royo, R. P. Stanley, M. Ilegems, K. Streubel, and K. H. Gulden, J. Appl. Phys. **91**, 2563 (2002).

[19] S. Yu. Karpov, Opt. Quant. Electron. **47**, 1293 (2015).

[20] N. Lobo Ploch, H. Rodriguez, C. Stölmacker, M. Hoppe, M. Lapeyrade, J. Stellmach, F. Mehnke, Tim Wernicke, A. Knauer, V. Kueller, M. Weyers, S. Einfeldt, and M. Kneissl, IEEE Trans. Electron. Devices **60**, 782 (2013).